Optically tunable metal-dielectric diffractive structures

Sylvain Chevalier,[1] Filippo Fabbri,[2] Khalid Lahlil,[1] Yves Lassailly,[1] Lucio Martinelli,[1] Thierry Gacoin,[1] and Jacques Peretti[1,*]

[1]*Laboratoire de Physique de la Matière Condensée, Ecole polytechnique, CNRS, Institut Polytechnique de Paris, F-91120 Palaiseau, France*
[2]*Centre for Nanoscience and Nanotechnology (C2N), CNRS, Université Paris Sud, Université Paris-Saclay, F-91120 Palaiseau, France*

(Received 9 May 2022; accepted 12 August 2022; published 12 September 2022)

Hybrid metal-polymer micropillar arrays are elaborated by solvent-assisted embossing techniques and subsequent gold deposition. The polymer is poly(methyl methacrylate) (PMMA) grafted with Disperse Red 1 (DR1) azobenzene derivatives. This photochromic material exhibits spectacular photomechanical properties. Under off-normal *p*-polarized illumination in the absorption band of the DR1, the metal-polymer hybrid micropillars bend in a direction determined by the light polarization. The deformation remains stable when the light excitation is turned off. The optically driven modification of the pillar shape allows us to tune the optical properties of the pillar arrays. Very large intensity changes are measured in the diffraction spectra at zero order (specular reflection), first order, and second order, with almost on and off switching of the diffraction efficiency. The photoinduced bending of the micropillars can be fully reversed by switching the linear light polarization to the orthogonal *s*-polarization state. This allows us to restore the initial optical properties of the pillar array. The polarization-controlled reversibility of the pillar deformation suggests a complex photoinduced deformation mechanism involving stress and stress release assisted by the change in the viscoelastic properties of the polymer under illumination in the absorption band of the DR1 chromophore.

DOI: 10.1103/PhysRevMaterials.6.095202

I. INTRODUCTION

Micro- and nanostructuration is a major route to produce materials and devices with tailored properties for various applications such as smart coatings [1]. A current challenge is to incorporate active materials which can respond to an external stimulus, either optical, electrical, magnetic, or mechanical, in order to control the structure shape and to tune the material or device properties. To address this issue, light-responsive materials are particularly attractive because optical stimuli enable noncontact operation, fast and easy addressability down to the submicron scale, compatibility with various environments, and selectivity through different parameters (wavelength, polarization, power, etc.). In this context, azobenzene-containing materials are under investigation for their specific ability to mechanically respond to light excitation [2–8]. Their photomechanical properties are related to the photoisomerization of the azobenzene units. When the chromophore exhibits a push-pull character, like the Disperse Red 1 (DR1) compound, illumination in the molecule absorption band induces repeated *trans-cis-trans* cycles which lead to spectacular deformation of the host material [2,3]. This photoinduced deformation involves several mechanisms: photoexpansion [9], light-induced change in mechanical properties [10–12], and polarization-directed mass motion [13–19]. Efficient structuration of the azobenzene-containing materials can thus be simply achieved by projection of an optical pattern. The photoinduced deformation process can be controlled over a wide scale range, from a few tens of nanometers [15] to several microns [19]. However, the produced pattern shapes are limited to rather smooth reliefs.

On the other hand, various embossing techniques were developed to pattern soft materials [20–25]. These techniques were, in particular, applied to azobenzene-containing polymers and allowed for the fabrication of micro- and nanostructures with large aspect ratios and abrupt shapes that cannot be elaborated by holographic inscription methods exploiting the photoinduced mass motion. The photomechanical response of the produced structures was then investigated, and spectacular modifications of the initial pattern shape due to the photoinduced mass motion were evidenced [26–30]. As for thin films, adjusting the illumination parameters, in particular the light polarization, allows controlling the pattern deformation. These photoactive structures showed potential applications as tunable diffractive devices [31], light-controlled hydrophobic layers [32,33], and active mechanical substrates in biology [34–36]. A further challenging issue is to associate the azobenzene-containing materials with nonphotoactive materials in order to elaborate a hybrid structure with tunable properties. Recent works reported on metal/azobenzene-containing material structures [26,37,38]. Although these studies showed the potentiality of this approach for designing devices with tailored optical and plasmonic properties, the tunability of the hybrid structure shape was not exploited.

In this paper, we report on the fabrication and study of metal/dielectric hybrid micropillar arrays which possess tunable optical properties. These micropillar arrays are obtained by solvent-assisted molding of an azobenzene-containing

*jacques.peretti@polytechnique.edu

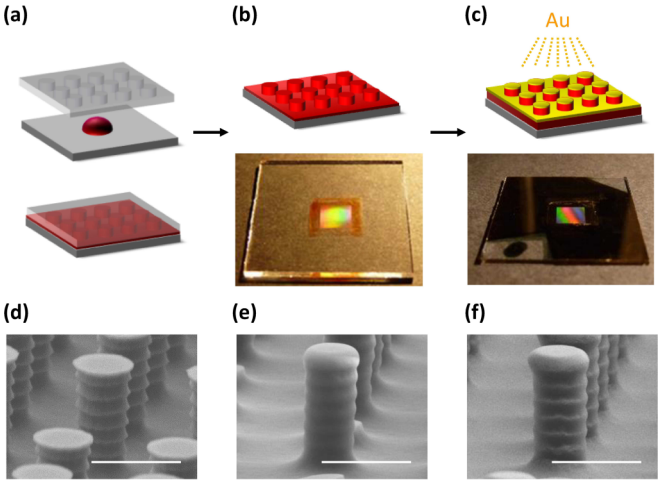

FIG. 1. (a) Schematic of the solvent-assisted embossing process of the PMMA-DR1 polymer dissolved in NMP using a PDMS mold. (b) and (c) PMMA-DR1 pillar array replicated on a $2.5 \times 2.5\,cm^2$ glass substrate before and after deposition of a 50 nm thick Au layer, respectively. (d)–(f) SEM images of a pillar array on the silicon master, of the bare PMMA-DR1 replicate, and of the metallized PMMA-DR1 replicate after deposition of the 50 nm thick Au layer. The pattern period is 3 μm, and the pillar diameter and height are, respectively, 1.2 and 2.5 μm. The scale bar on the SEM images is 2 μm.

polymer and subsequent metal deposition by evaporation under vacuum. The photomechanical properties of the azobenzene-containing material enable us to control the deformation of the pillars by an optical stimulus. We demonstrate that the photoinduced change in the pillar shape allows for the fine tuning of the optical properties of the metal/dielectric pillar array. The process is shown to be almost fully reversible by using an appropriate sequence of polarized illumination. Simulations of the optical properties of the metal/dielectric structures before and after photoinduced deformation are performed based on the rigorous coupled-wave analysis (RCWA). Numerical results show good agreement with the experimental data.

II. SAMPLE PREPARATION

Our fabrication process of hybrid metal/photoactive polymer structures is schematized in Fig. 1. It is based on solvent-assisted embossing with a PDMS (polydimethylsiloxane) stamp, a well-known approach for the replication of patterns on soft materials [20–25]. Arrays of micro- and nanostructures with high aspect ratios can be elaborated in this way [33].

The PDMS stamps were prepared from silicon masters fabricated by a customized Bosch process. A Bosch process is a dry-etching technique that consists of cycles alternating isotropic etching under SF_6 plasma and sidewall passivation/protection using C_4F_8 plasma. This method inherently induces surface scalloping, which here can be as large as 200 nm. It is a direct consequence of the alternating deposition and etching cycles and depends on the timing of the steps in each cycle and on the etching rate. A Rapier tool was used, with 2.5kW of 13.56 MHz rf power. The temperature of the wafer was controlled using an electrostatic chuck. An oxygen cleaning procedure was performed to remove polymers from the sidewalls of the reactor, minimizing contamination. The details of the process were reported elsewhere [39]. A silanization treatment of the patterned Si surface was subsequently performed with TMCS (trimethylchlorosilane) in the gaseous phase in order to minimize the adhesion of the PDMS stamp to the Si surface when unmolding. The PDMS solution was prepared by mixing a PDMS prepolymer and an initiator (Memorive RTV615) with a 10:1 weight ratio and subsequently outgassed under vacuum. The outgassed solution was then carefully poured onto the patterned master to prevent the generation of bubbles. Finally, the PDMS solution was cured at 60 °C in an oven for 3 *h*. After complete reticulation, the PDMS stamp was detached from the Si master.

The PDMS stamp was then gently put on a small droplet of an azopolymer solution deposited on a freshly cleaned glass substrate [Fig. 1(a)]. After drying the solvent at 50 °C for 12 h, the PDMS was peeled off, leaving the azopolymer transferred pattern on the glass substrate [Fig. 1(b)]. The azopolymer is prepared from a $30\,mg/mL$ solution of PMMA-DR1 (polymethyl-methacrylate-co-Disperse Red 1, from Sigma Aldrich) dissolved in NMP (*N*-methyl-2-pyrrolidone).

Figures 1(d) and 1(e) show scanning electron microscope (SEM) images of the pillars on the silicon master and on the processed PMMA-DR1 layer, respectively. The period of the pillar array is 3 μm, and the characteristic dimensions of the PMMA-DR1 cylindrical pillars are a 1.2 μm diameter and 2.5 μm height, leading to an aspect ratio slightly larger than 2. SEM analysis of the silicon masters, the PDMS stamps, and the PMMA-DR1 structured films was performed for various pillar arrays with different characteristic dimensions to investigate the quality of the pattern transfer. We observed a good match between the geometrical parameters of the silicon master pattern, the PDMS mold, and the PMMA DR1 replicate, leading to the conclusion that the technique is robust for a large range of structure dimensions. Annular structures observed on the sidewalls of the silicon pillars and of the PMMA-DR1 replica are due to the successive steps of the Bosch lithography process.

A 50 nm gold layer is deposited by evaporation in vacuum at normal incidence on the patterned PMMA-DR1 thin films [Fig. 1(c)]. In this configuration, only the top of the PMMA-DR1 pillars and the surface of the residual PMMA-DR1 base layer are covered with gold, while the pillar sidewalls mainly remain bare, except for the annular protrusions induced by the Bosch lithography process [Fig. 1(f)].

III. PHOTOMECHANICAL RESPONSE OF PHOTOACTIVE PILLAR ARRAYS

The DR1 azobenzene derivative exhibits a blue absorption band. Illumination in this band efficiently excites the photoisomerization between *trans* and *cis* forms. In the following, we use a laser emitting at 488 nm, very close to the DR1 absorption peak, to study the photomechanical response of the pillar arrays. In all experiments presented here, samples are excited with an incidence angle of 45°. Since the photoinduced deformation of azobenzene-containing polymers is

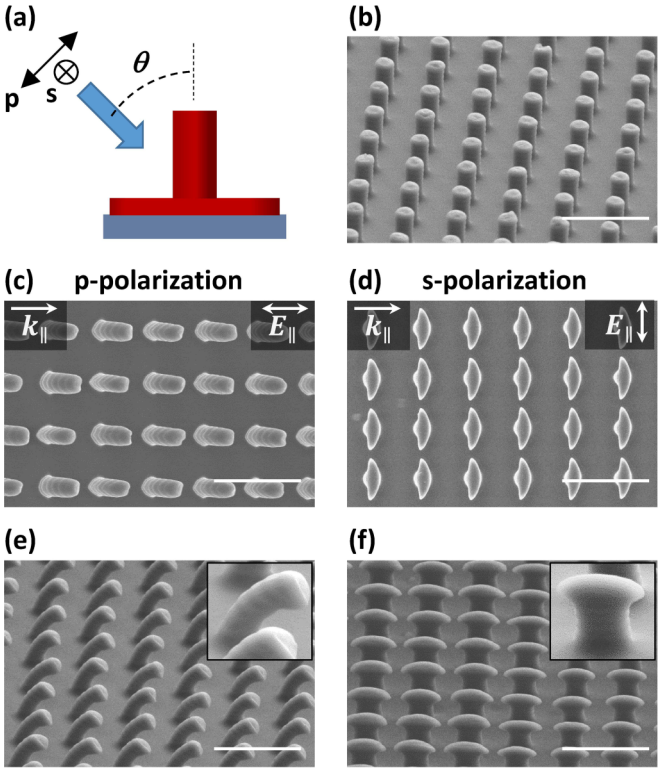

FIG. 2. (a) Schematic of the pillar illumination geometry. (b) SEM image of the bare PMMA-DR1 pillar array. (c) and (e) Top and oblique views of the same pillar array after 10 min illumination by a *p*-polarized laser beam of wavelength 488 nm and power density of 2 mW/mm^2, with an incidence angle of 45°. (d) and (f) Same as (c) and (e) for illumination with *s*-polarized light. The scale bar is 5 μm. The orientation of the light wave vector and electric field in-plane components are indicated. Insets in (e) and (f) show a zoom of the pillar after deformation.

known to be a polarization-directed process, we will study the photomechanical response of the pillar structures for linear *p*- and *s*-polarization states.

Figure 2 shows the SEM images of the micropillar array before and after 10 min illumination with 2 mW/mm^2 power density of the 488 nm laser.

When the light is *p* polarized, the pillars are seen to bend, which was already recently reported [40]. A slight change in the pillar top surface shape is observed. The microscopic origin of the photoinduced deformation of azobenzene-containing materials has not been fully elucidated, but as already mentioned, it is known to involve an efficient mass migration process mainly governed by the light polarization pattern [14,15,17,41,42]. In the present experiment, the pillar bending is directed by the light polarization. When the light polarization is rotated away from the *p*-polarization direction, the pillar bending direction is also rotated, and the bending efficiency decreases.

When the light is *s* polarized, the pillar does not bend. Instead, a symmetric deformation of the pillar occurs, predominantly on the top face of the pillar, along the light polarization direction [Figs. 2(d) and 2(f)]. Since the deformation originates from the photoinduced mass motion directed by the light polarization, *s* polarization can induce only a

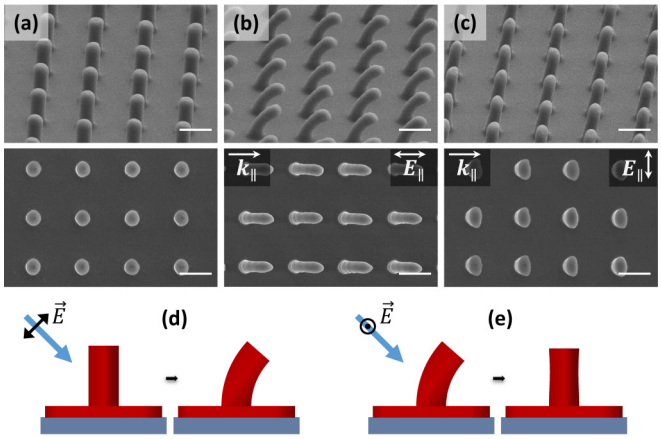

FIG. 3. SEM images (oblique and top views with a 2 μm scale bar) of the pillar array (a) before illumination, (b) after 10 min illumination with *p*-polarized light, and (c) after subsequent 10 min illumination with *s*-polarized light. The laser excitation settings were identical to those of Fig. 2. (d) Under illumination with *p*-polarized light, pillars bend. (e) Under subsequent illumination with *s*-polarized light pillars unbend and recover their initial vertical shape.

symmetric deformation perpendicular to the pillar axis. The resulting deformation is thus not a bending of the pillar but appears as a transverse stretch which is more efficient on the free flat top surface of the pillar than on the curved pillar sidewall.

Therefore, *p*- and *s*-polarized illuminations induce completely different deformations. However, surprisingly, pillars that were bent by *p*-polarized illumination are seen to unbend and recover their initial vertical shape when subsequently illuminated with *s*-polarized light. This is shown in Fig. 3, which presents scanning electron microscopy images of the same pillar structure before illumination, after 10 min illumination with *p*-polarized light, and after subsequent 10 min illumination with *s*-polarized light.

Photoinduced bending and unbending at a macroscopic scale were demonstrated in liquid crystal elastomer incorporating azobenzene moieties [43]. In that case, the deformation was fully reversible as it was related to single photoisomerization processes of almost bistable azobenzene derivatives: the transition from *trans* to *cis* states was induced with one wavelength and produced the film bending, and the back transition from *cis* to *trans* states was induced with another wavelength and produced the unbending of the film. In our case, the deformation process is much more complex because it involves repeated *trans-cis-trans* photoisomerization cycles and polarization-directed mass migration. Previous works have already shown that the deformation induced by linearly polarized light in pillars of materials containing azobenzene push-pull derivatives can be partially reversed by a subsequent illumination with the orthogonal polarization [30,31]. However, this was achieved in the specific geometry where the sample was illuminated in normal incidence. In this case, the two orthogonal polarizations should both produce a stretch of the pillar top surface but along orthogonal directions. If the volume is conserved, one can reasonably assume that

subsequent stretches along two orthogonal directions may compensate each other, at least to first order. In contrast, in the case of off-normal incidence, which we use, illuminations with *p* and *s* polarizations do not induce equivalent deformations (Fig. 3), and it is hardly conceivable that the bending induced by *p*-polarized illumination may be reversed by a subsequent stretch in the orthogonal direction induced by *s*-polarized illumination. We thus propose a different explanation. Illumination with *p*-polarized light produces at the same time a drop in the PMMA-DR1 viscosity [12] and a mass motion along the illuminated sidewall of the pillar. Since the absorption length of the exciting light in the PMMA-DR1 is smaller (200 nm) than the pillar diameter (1200 nm), the off-normal illumination produces a dissymmetric deformation which results in the pillar bending and induces a stress across the pillar. When *p*-polarized illumination is turned off, the material viscosity jumps back to its initial value, which is too high for the stress to relax and the pillar deformation is "frozen." Under subsequent *s*-polarized illumination, viscosity drops down again, and the stress produced under *p*-polarized illumination is released, which results in the pillar unbending.

It has to be noted that, according to this mechanism, the photoinduced deformation of the pillars is governed by the illumination of the pillar sidewall. Therefore, in the case of the metal-dielectric pillar arrays obtained by gold evaporation at normal incidence, since the pillars exhibit sharp edges and the pillar sidewalls are thus not metallized [Fig. 1(f)], it might be expected that the photomechanical properties of these structures are preserved. This contrasts with previous studies of metal-dielectric structures consisting of gold-covered azopolymer thin films [37,38]. In these works, the photoactive polymer was patterned by holographic techniques to produce surface relief gratings prior to the metal deposition. But once the layer was deposited all over the patterned azobenzene-containing polymer, the photomechanical properties of the photoactive material were inhibited, and further photoinduced deformation of the structure was impossible. The optical properties of the device were thus not tunable.

When illuminating the metallized pillar array with *p*-polarized light, at an incidence angle of 45°, bending of the hybrid pillars is observed [Fig. 4(b)]. Under subsequent illumination with *s*-polarized light, the gold-covered pillars unbend and almost completely recover their initial shape, as was observed on bare PMMA-DR1 structures [Fig. 4(c)]. After the *p*+*s* illumination sequence, the pillars appear to be only a few percent shorter than before illumination. As expected, the photomechanical response of the photoactive structure is thus preserved, although the photoinduced deformation process is significantly less efficient than on the nonmetallized pillar array. Indeed, a deformation similar to that of the nonmetallized pillar structure is obtained with the same illumination time of 10 min but with a power density of 20 mW/mm^2, i.e., 10 times higher. This might be due to slight metallization of the pillar sidewall in spite of the normal incidence geometry of the gold evaporation. Note that, since a 50 nm thick gold film deposited on PMMA-DR1 precludes the photoinduced mass transport in the photoactive polymer, the gold-covered surfaces, at the top of the pillars and on the residual base PMMA-DR1 layer, are not modified by the illumination.

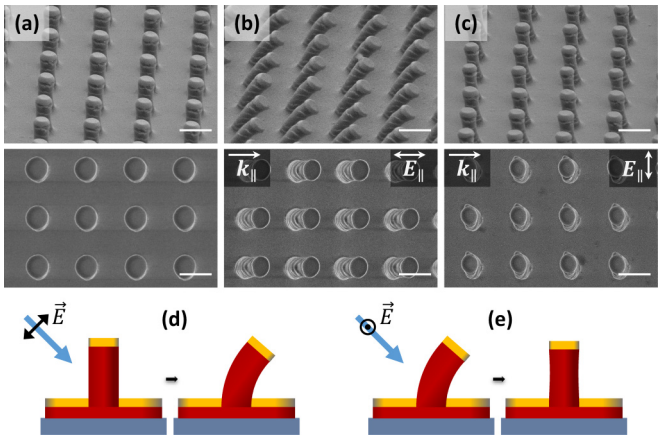

FIG. 4. SEM images (oblique and top views with 2 μm scale bar) of the pillar array coated with 50 nm of gold (a) before illumination, (b) after 10 min illumination with *p*-polarized light, and (c) after subsequent 10 min illumination with *s*-polarized light. The illumination power density was 20 mW/mm^2. (d) Excitation with *p*-polarized light induces pillar bending. (e) Under subsequent illumination with *s*-polarized light pillars unbend and recover their initial vertical shape.

IV. TUNABLE OPTICAL PROPERTIES OF PHOTOACTIVE HYBRID PILLAR ARRAYS

Micro- and nanostructured metal/dielectric hybrid systems are widely studied and used for optics and plasmonics applications [44,45]. Their properties are governed by the geometrical characteristics of the pattern at the micro- or nanometer scale. Modifying the pattern shape should therefore allow for tuning their optical properties.

The change in the reflectivity spectrum of the gold-covered sample during the photoinduced pillar deformation is shown in Fig. 5. In this experiment, an unpolarized collimated white light beam with weak power density (a few microwatts per square millimeter) is used as a probe. The reflected light is analyzed by a spectrophotometer. The incidence angle of the white light probe beam is fixed at 10°. The specular reflected beam at −10° is focused on the spectrophotometer entrance slit with a convergent lens which matches the spectrophotometer aperture. The measured reflectance spectrum is normalized by the white light source spectrum measured with the same spectrophotometer. The structure is photoexcited with a low 488 nm laser power density of 0.25 mW/mm^2 at an incidence angle of 45°. The laser beam is *p* polarized for the first 120 min and *s* polarized for the following 120 min.

Before excitation with the 488 nm laser, the reflectivity spectrum between 400 and 950 nm shows large modulations due to the interferences between the light reflected by the gold layer at the top and bottom of the pillar [Fig. 5(b)]. The spectral positions of the modulation extrema essentially depend on the pillar height (here 2.5 μm), and the modulation amplitude depends on the filling factor (the ratio between the pillar top surface area and the base surface area). The low reflectivity in the blue range is due to the decrease in the gold

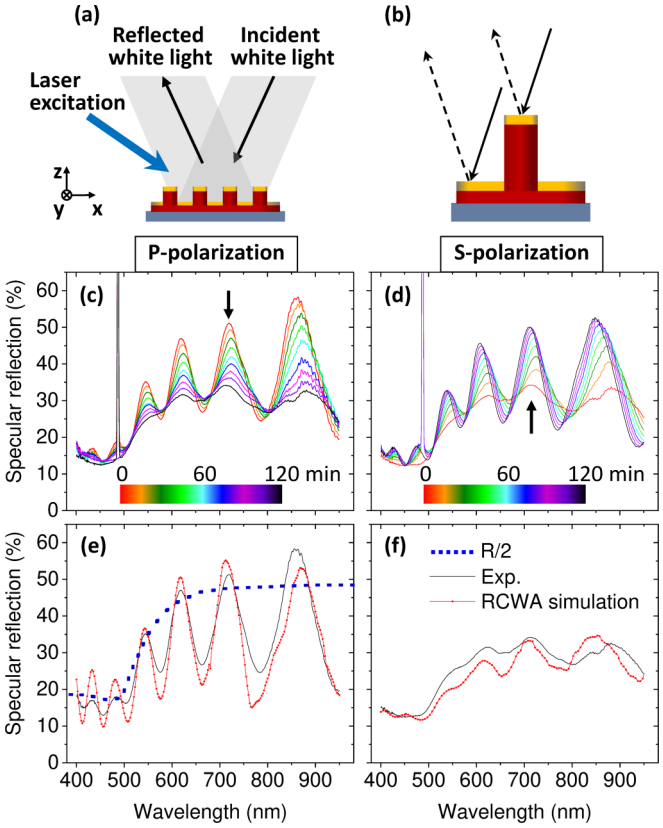

FIG. 5. (a) Schematics of the measurement configuration of the reflectivity spectrum during light excitation of the hybrid pillar array. The incidence angle of the probe white light is 10°. Specular reflection is collected by the spectrophotometer. The sample is excited with the 488 nm laser beam with power density of 0.25 mW/mm^2 at an incidence angle of 45°. (b) Schematic of the interfering beams scattered on the pillar top surface and on the base plane. (c) Evolution of the reflectivity spectrum during *p*-polarized illumination of the pillar array. (d) Reverse evolution of the reflectivity spectrum during subsequent *s*-polarized excitation inducing the pillar unbending. In (c) and (d), the color code indicates the exposure time to the excitation laser. The peak at 488 nm is due to the diffusion of the excitation laser. (e) and (f) Comparison of the experimental data with RCWA simulations of the reflection spectra of the initial and bent pillar arrays, respectively. In (e), as a reference, the dotted blue curve represents the reflectance spectra *R* of the flat 50 nm thick gold layer away from the pillar structure (for the sake of graph readability *R*/2 is plotted).

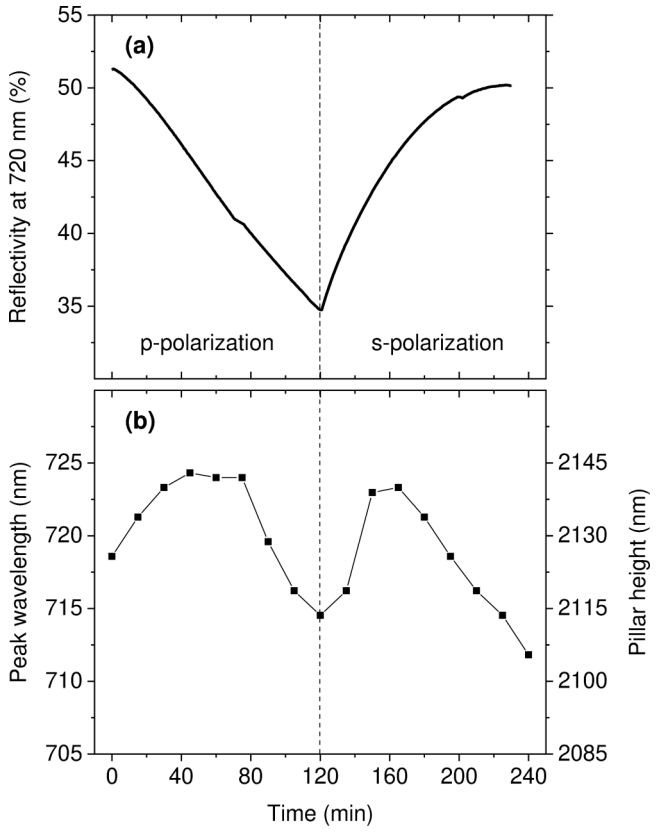

FIG. 6. Evolution of (a) the reflected intensity and (b) peak wavelength of the constructive interference feature indicated by the arrows in the reflectivity spectra in Figs. 5(c) and 5(d) during *p*- and subsequent *s*-polarized illumination. The left axis in (b) indicates the pillar height, which can be deduced from the position of the interference extrema in the reflectivity spectrum.

layer reflectivity. In Fig. 5(e), the reflectance spectrum *R* of the flat 50 nm thick gold layer away from the pillar structure is plotted as a reference (dotted blue line).

During illumination with the *p*-polarized blue laser beam, progressive destruction of the interferences is observed. This evolution is due to the pillar bending. After 120 min of illumination, the modulations in the reflectivity spectrum have almost completely disappeared. We performed RCWA calculations of the reflectivity spectrum of the metallized sample, using the values of the geometrical parameters of the pillars deduced from SEM observations. The refractive indices of the materials in the probed spectral range were measured (by ellipsometry) for PMMA-DR1 and taken from the literature for gold [46]. Good agreement is found between the simulations and the experimental results [Figs. 5(e) and 5(f)].

After the modulations in the reflectivity spectrum have almost completely vanished, the blue laser beam polarization is switched to *s* polarization in order to induce unbending of the pillars. As a result, the intensity modulations show up again on the reflectivity spectrum. We thus succeed in reversibly modifying the structure shape by an optical stimulus and tuning this way the optical properties of the hybrid pillar array. Note that, when *p*-polarized illumination is extended well beyond the suppression of the reflectivity spectrum modulation, the deformation of the pillars still continues but cannot be reversed anymore by subsequent *s*-polarized illumination.

The evolution of the shape of the structures during *p*- and *s*-polarized illumination can be estimated by analyzing the change in the reflectivity spectrum. Figure 6(a) shows the variation of the reflectivity at 720 nm, which corresponds to a maximum (constructive interference) in the reflectivity spectrum during the *p*- and *s*-polarized illumination sequence. The variation of the peak wavelength of the corresponding maximum is plotted in Fig. 6(b). The intensity is somehow related to an effective filling factor of the structure, while the spectral position of the extremum is related to the pillar height. Under *p*-polarized illumination, the reflected intensity around

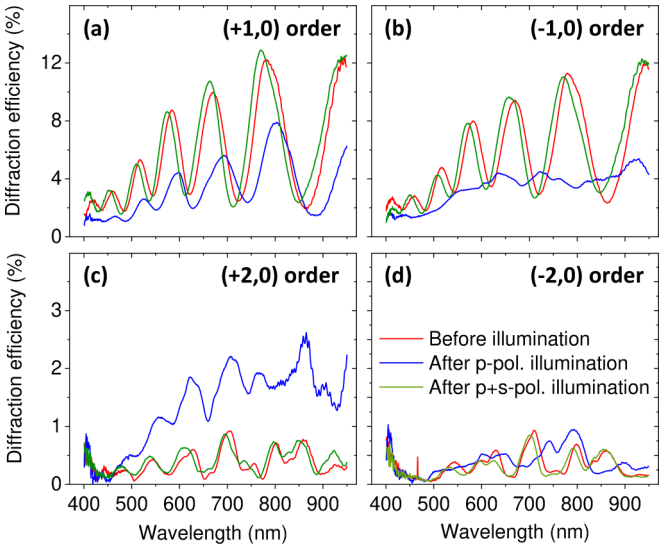

FIG. 7. Diffraction spectra of the first $(\pm 1, 0)$ and second $(\pm 2, 0)$ orders of the gold-covered pillar array before illumination (red curve), after 120 min *p*-polarized illumination (blue curve), and after subsequent 120 min *s*-polarized illumination (green curve).

720 nm strongly decreases due to the diminution of the light scattered in the specular direction by the top of the pillars when the pillars bend. Interestingly, the spectral position of the reflectivity maximum only slightly changes, by less than 2%, indicating that the height of the pillars remains almost the same. This shows that a moderate photoinduced deformation of the pillars produces a large change in the reflectivity spectrum.

Note that moderate deformations are favorable to achieve reversibility. When switching the excitation polarization from *p* to *s*, the reflectivity (i.e., the interference modulation amplitude) immediately starts to rise again and reaches a value of 50% very close to the initial one of 52% (before *p*-polarized illumination). The illumination times are similar for suppressing the interference modulation with the *p*-polarized illumination and for restoring it with *s*-polarized illumination. During the unbending process with *s*-polarized excitation, a 10 nm redshift of the reflectivity maximum position from 715 to 725 nm is observed which is followed by a 14 nm blueshift. This is due first to the slight increase in the tilted pillar effective height when unbending and then to the slight diminution of pillar height after unbending due to the transverse stretch of the pillars induced by *s*-polarized illumination (see Figs. 3 and 4).

The deformation of the pillars is also expected to modify the diffraction properties of the pillar array. Since the photoinduced pillar deformation under *p*-polarized illumination introduces both an asymmetry and an anisotropy in the structure, the change in the diffraction efficiency must be different for the different diffraction orders. We have measured the diffraction efficiency spectrum of the first and second diffraction orders (Fig. 7). In this experiment, the probe white light beam illuminates the structure at normal incidence, and the spectrum of each diffraction order is measured by detecting the light collected in the spectrophotometer as a function of the detection angle. The different diffraction orders are

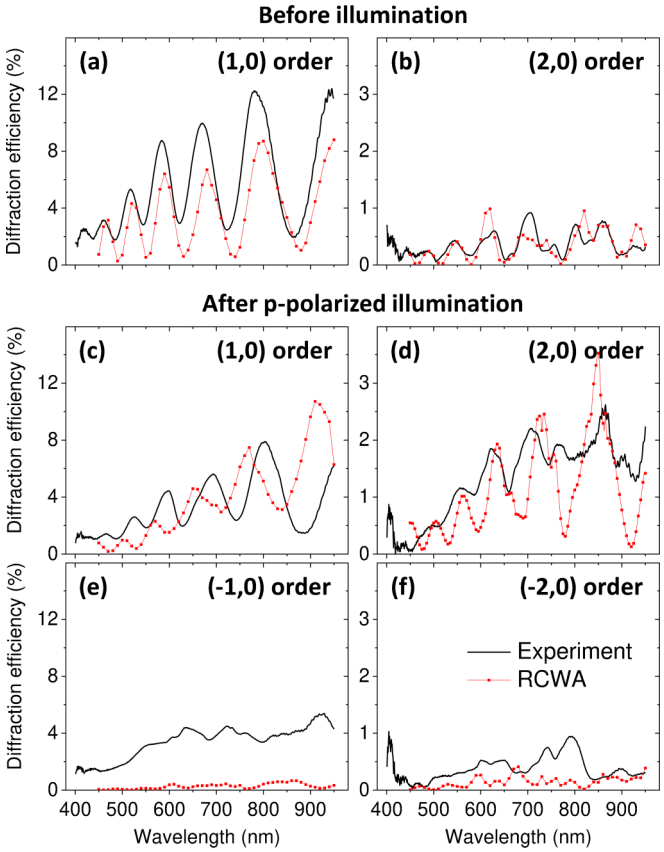

FIG. 8. (a) First and (b) second diffraction order spectra of the 50 nm gold-covered sample before illumination: experiment (black curve) and RCWA simulation (red curve). Only positive orders are shown due to the system symmetry. (c) and (d) Same as (a) and (b) after *p*-polarized illumination. (e) and (f) Same as (c) and (d) for negative first and second diffraction orders. The pillar bending produces an asymmetry between opposite diffraction orders.

labeled (x, y) according to their respective coordinates in the xy plane of observation, parallel to the sample surface plane. The incidence plane of the excitation blue laser is the xz plane so that the $(x, 0)$ diffraction orders are in the plane of the pillar deformation. In the initial state, strong interference modulations are observed in the spectrum of the first diffraction orders, like in the specular reflection spectrum. The efficiency of the second diffraction orders is one order of magnitude lower and exhibits a more complex interference modulation feature in the probed spectral range. Symmetric diffraction orders $(\pm x, 0)$ exhibit similar diffraction efficiency spectra. After a *p*-polarized illumination, the change in the diffraction efficiency spectrum strongly depends on the order index. The interference modulations in the efficiency spectrum of the (1,0) order are reduced by about a factor of 2, while they almost completely vanish for the $(-1, 0)$ order. The (2,0) order shows a large increase in efficiency, while the $(-2, 0)$ order spectrum is only slightly affected by the photodeformation of the pillar array and remains weak. Illumination with *s*-polarized excitation almost restores the initial diffraction spectra. In Fig. 8, these experimental results are compared with RCWA simulations. Before the photoinduced pillar deformation very good agreement is obtained, as

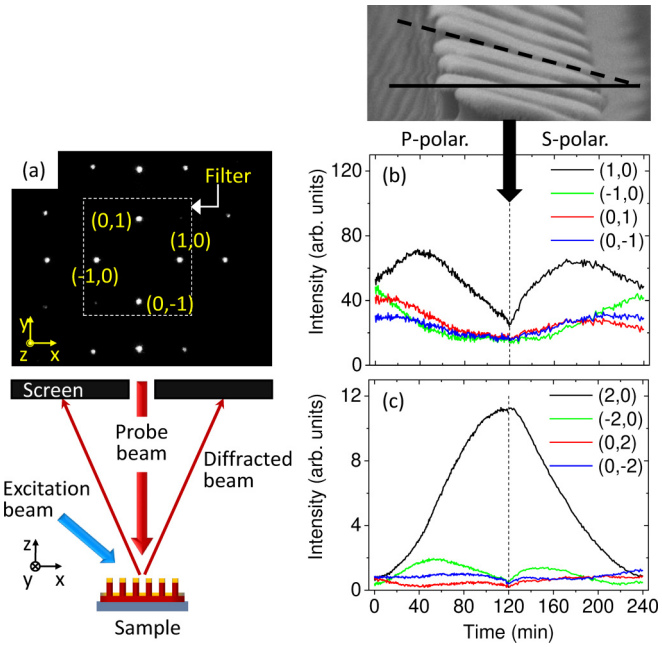

FIG. 9. (a) Schematic of the optical setup for measuring the intensity of the diffraction orders of the metallized pillar array as a function of photoexcitation time. The probe beam of 635 nm wavelength impinges the sample at normal incidence. Diffracted beams are projected on a screen. The diffracted pattern is recorded by a CCD camera. A neutral filter (dashed square) attenuates the first diffraction orders by a factor of 30 in order to avoid saturation of the camera. A linearly polarized blue laser beam with a 488 nm wavelength and 0.25 mW/mm^2 power density excites the sample with a 45° incidence angle. Evolution of the intensity of the (b) first and (c) second diffraction orders during excitation of the structure with p polarization and subsequently with s polarization. A SEM image of the bent pillars after p-polarized illumination is shown in (b).

previously observed. After the photoinduced pillar deformation, the slight discrepancies between the calculated and measured diffraction spectra are due to the fact that the actual shape of the bent pillars is not easy to reproduce in basic RCWA simulations. In particular, the positions of the interference extrema are very much dependent on the pillar height, which, as we have seen, may change nonmonotonously during the deformation process. However, the RCWA simulations reproduce quite well the trend in the change in the diffraction efficiency for the different orders.

The evolution of the different diffraction orders of the two-dimensional pillar array can be measured during the photoinduced deformation process. In this experiment [Fig. 9(a)], a 635 nm probe laser beam, out of the DR1 absorption band, impinges the sample surface at normal incidence, and the diffraction pattern is projected on a screen. The intensities of the different diffraction orders are recorded by a CCD camera. A neutral filter is placed at the center of the screen in order to attenuate by a factor of 30 the first diffraction orders: $(0, \pm 1)$, $(\pm 1, 0)$, and $(\pm 1, \pm 1)$, avoiding saturation of the camera. The sample is excited with a 488 nm laser power density of 0.25 mW/mm^2 at an incidence angle of 45° in the xz plane.

Clearly, the photoinduced pillar deformation mainly affects the $(+1, 0)$ and $(+2, 0)$ orders [black curves in Figs. 9(b) and 9(c)]. The $(+1, 0)$ order intensity first increases, reaches a maximum value, and then decreases monotonously. At the same time, the $(+2, 0)$ order intensity increases spectacularly by a factor of 10, while the $(-2, 0)$ order remains almost unchanged. The variations of the $(+1, 0)$ and $(+2, 0)$ orders can be explained by a blazinglike effect. Bending of the pillars first improves the efficiency of the $(+1, 0)$ order up to an optimum effective blazing angle which is reached after about 40 min of illumination. Beyond this deformation, the diffraction efficiency decreases. For the $(+2, 0)$ diffraction order, the optimum effective blazing angle is about twice as large, and the intensity reaches a maximum value after about 115 min of illumination. From SEM observations (top image in Fig. 9), we measure a tilt of the pillar top surface of about 15° after 120 min of p-polarized illumination. For a grating with a 3 μm period, blazed at 635 nm, the expected blaze angle is about 6° at first order and about 12° at second order, which is in good agreement with the observed tilt of about 15°. Note that, after switching the excitation from p to s polarization, the deformation is reversed, and the initial diffraction pattern is progressively almost fully restored within a similar excitation time. However, as clearly seen in Fig. 9(c), the kinetics of the change in the diffraction efficiency under p-polarized excitation and of the reverse process under s-polarized excitation are not identical. The variation with exposure time of the $(+2, 0)$ diffraction order efficiency shows first a sigmoidlike increase under p excitation, which is characteristic of the usual PMMA-DR1 photoinduced deformation process, and then an exponential-like decrease under s excitation, which suggests a relaxation process.

V. CONCLUSION

In conclusion, we have demonstrated that azobenzene-containing materials can be used to elaborate micro- and nanostructured hybrid metal/dielectric devices with tunable optical properties. Micropillar arrays of PMMA-DR1 were prepared by solvent-assisted embossing. A thin Au layer was deposited by evaporation under vacuum. Areas of the embossed azopolymer structure which were unexposed to the ballistic metal flux keep their photomechanical properties, and photoinduced deformation of the hybrid structure remains possible under light excitation at oblique incidence. The direction of the deformation can be controlled by the incident light polarization. The optical properties (reflection and diffraction spectra) of the pillar arrays measured during the photoinduced deformation process exhibit very large changes. The reversibility of the photoinduced deformation is achieved thanks to a proper illumination sequence with polarized light which allows us to recover the initial optical properties of the structure. The proposed approach is based on a very simple technological process and allows for the fabrication of a wide range of hybrid micro- and nanostructures which could potentially lead to the development of tunable optical and plasmonic devices.

[1] S. B. Ulaeto, J. K. Pancrecious, T. P. D. Rajan, and B. C. Pai, *Smart coatings*, in *Noble Metal-Metal Oxide Hybrid Nanoparticles* (Elsevier, Amsterdam, 2018), pp. 341–372.

[2] P. Rochon, E. Batalla, and A. Natansohn, Optically induced surface gratings on azoaromatic polymer films, Appl. Phys. Lett. **66**, 136 (1995).

[3] D. Kim, S. Tripathy, L. Li, and J. Kumar, Laser-induced holographic surface-relief gratings on nonlinear-optical polymer-films, Appl. Phys. Lett. **66**, 1166 (1995).

[4] N. Viswanathan, D. Kim, S. Bian, J. Williams, W. Liu, L. Li, L. Samuelson, J. Kumar, and S. Tripathy, Surface relief structures on azo polymer films, J. Mater. Chem. **9**, 1941 (1999).

[5] J. Delaire and K. Nakatani, Linear and nonlinear optical properties of photochromic molecules and materials, Chem. Rev. **100**, 1817 (2000).

[6] A. Natansohn and P. Rochon, Photoinduced motions in azo-containing polymers, Chem. Rev. **102**, 4139 (2002).

[7] Z. Mahimwalla, K. G. Yager, J.-I. Mamiya, A. Shishido, A. Priimagi, and C. J. Barrett, Azobenzene photomechanics: Prospects and potential applications, Polym. Bull. (Heidelberg, Ger.) **69**, 967 (2012).

[8] T. Taniguchi, T. Asahi, and H. Koshima, Photomechanical azobenzene crystals, Crystals **9**, 437 (2019).

[9] D. Garrot, Y. Lassailly, K. Lahlil, J. P. Boilot, and J. Peretti, Real-time near-field imaging of photoinduced matter motion in thin solid films containing azobenzene derivatives, Appl. Phys. Lett. **94**, 033303 (2009).

[10] N. Mechau, D. Neher, V. Borger, H. Menzel, and K. Urayama, Optically driven diffusion and mechanical softening in azobenzene polymer layers, Appl. Phys. Lett. **81**, 4715 (2002).

[11] K. G. Yager and C. J. Barrett, Photomechanical surface patterning in azo-polymer materials, Macromolecules **39**, 9320 (2006).

[12] L. Sorelli, F. Fabbri, J. Frech-Baronet, A.-D. Vu, M. Fafard, T. Gacoin, K. Lahlil, L. Martinelli, Y. Lassailly, and J. Peretti, A closer look at the light-induced changes in the mechanical properties of azobenzene-containing polymers by statistical nanoindentation, J. Mater. Chem. C **3**, 11055 (2015).

[13] C. Barrett, A. Natansohn, and P. Rochon, Mechanism of optically inscribed high-efficiency diffraction gratings in azo polymer films, J. Phys. Chem. **100**, 8836 (1996).

[14] N. Viswanathan, S. Balasubramanian, L. Li, S. Tripathy, and J. Kumar, A detailed investigation of the polarization-dependent surface-relief-grating formation process on azo polymer films, Jpn. J. Appl. Phys. **38**, 5928 (1999).

[15] N. Landraud, J. Peretti, F. Chaput, G. Lampel, J. Boilot, K. Lahlil, and V. Safarov, Near-field optical patterning on azo-hybrid sol-gel films, Appl. Phys. Lett. **79**, 4562 (2001).

[16] M. Helgert, L. Wenke, S. Hvilsted, and P. Ramanujam, Surface relief measurements in side-chain azobenzene polyesters with different substituents, Appl. Phys. B **72**, 429 (2001).

[17] P. Karageorgiev, D. Neher, B. Schulz, B. Stiller, U. Pietsch, M. Giersig, and L. Brehmer, From anisotropic photo-fluidity towards nanomanipulation in the optical near-field, Nat. Mater. **4**, 699 (2005).

[18] F. Fabbri, D. Garrot, K. Lahlil, J. P. Boilot, Y. Lassailly, and J. Peretti, Evidence of two distinct mechanisms driving photoinduced matter motion in thin films containing azobenzene derivatives, J. Phys. Chem. B **115**, 1363 (2011).

[19] S. L. Oscurato, M. Salvatore, F. Borbone, P. Maddalena, and A. Ambrosio, Computer-generated holograms for complex surface reliefs on azopolymer films, Sci. Rep. **9**, 6775 (2019).

[20] E. Kim, Y. Xia, and G. Whitesides, Polymer microstructures formed by molding in capillaries, Nature (London) **376**, 581 (1995).

[21] E. Kim, Y. Xia, and G. Whitesides, Micromolding in capillaries: Applications in materials science, J. Am. Chem. Soc. **118**, 5722 (1996).

[22] X. Zhao, Y. Xia, and G. Whitesides, Fabrication of three-dimensional micro-structures: Microtransfer molding, Adv. Mater. **8**, 837 (1996).

[23] P. Yang, T. Deng, D. Zhao, P. Feng, D. Pine, B. Chmelka, G. Whitesides, and G. Stucky, Hierarchically ordered oxides, Science **282**, 2244 (1998).

[24] C. Bulthaup, E. Wilhelm, B. Hubert, B. Ridley, and J. Jacobson, All-additive fabrication of inorganic logic elements by liquid embossing, Appl. Phys. Lett. **79**, 1525 (2001).

[25] C. Martin and I. Aksay, Microchannel molding: A soft lithography-inspired approach to micrometer-scale patterning, J. Mater. Res. **20**, 1995 (2005).

[26] S. Lee, J. Shin, Y.-H. Lee, S. Fan, and J.-K. Park, Directional photofluidization lithography for nanoarchitectures with controlled shapes and sizes, Nano Lett. **10**, 296 (2010).

[27] H. S. Kang, S. Lee, and J.-K. Park, Monolithic, hierarchical surface reliefs by holographic photofluidization of azopolymer arrays: Direct visualization of polymeric flows, Adv. Funct. Mater. **21**, 4412 (2011).

[28] S. Lee, H. S. Kang, A. Ambrosio, J.-K. Park, and L. Marrucci, Directional superficial photofluidization for deterministic shaping of complex 3d architectures, ACS Appl. Mater. Interfaces **7**, 8209 (2015).

[29] H. S. Kang, S. Lee, J. Choi, H. Lee, J.-K. Park, and H.-T. Kim, Light-induced surface patterning of silica, ACS Nano **9**, 9837 (2015).

[30] F. Pirani, A. Angelini, F. Frascella, R. Rizzo, S. Ricciardi, and E. Descrovi, Light-driven reversible shaping of individual azopolymeric micro-pillars, Sci. Rep. **6**, 31702 (2016).

[31] Y. Gritsai, L. M. Goldenberg, and J. Stumpe, Efficient single-beam light manipulation of 3d microstructures in azobenzene-containing materials, Opt. Express **19**, 18687 (2011).

[32] S. L. Oscurato, F. Borbone, P. Maddalena, and A. Ambrosio, Light-driven wettability tailoring of azopolymer surfaces with reconfigured three-dimensional posts, ACS Appl. Mater. Interfaces **9**, 30133 (2017).

[33] J. Choi, W. Jo, S. Y. Lee, Y. S. Jung, S.-H. Kim, and H.-T. Kim, Flexible and robust superomniphobic surfaces created by localized photofluidization of azopolymer pillars, ACS Nano **11**, 7821 (2017).

[34] C. Rianna, M. Ventre, S. Cavalli, M. Radmacher, and P. A. Netti, Micropatterned azopolymer surfaces modulate cell mechanics and cytoskeleton structure, ACS Appl. Mater. Interfaces **7**, 21503 (2015).

[35] C. Rianna, L. Rossano, R. H. Kollarigowda, F. Formiggini, S. Cavalli, M. Ventre, and P. A. Netti, Spatio-temporal control of dynamic topographic patterns on azopolymers for cell culture applications, Adv. Funct. Mater. **26**, 7572 (2016).

[36] F. A. Pennacchio, C. Fedele, S. De Martino, S. Cavalli, R. Vecchione, and P. A. Netti, Three-dimensional microstructured azobenzene-containing gelatin as a photoactuable cell confining system, ACS Appl. Mater. Interfaces **10**, 91 (2018).

[37] R. J. Moerland, J. E. Koskela, A. Kravchenko, M. Simberg, S. van der Vegte, M. Kaivola, A. Priimagi, and R. H. A. Ras, Large-area arrays of three-dimensional plasmonic subwavelength-sized structures from azopolymer surface-relief gratings, Mater. Horiz. **1**, 74 (2014).

[38] H. S. Kang, S. Lee, S.-A. Lee, and J.-K. Park, Multilevel micro/nanotexturing by three-dimensionally controlled photofluidization and its use in plasmonic applications, Adv. Mater. **25**, 5490 (2013).

[39] E. Herth, S. Edmond, D. Bouville, J. L. Cercus, F. Bayle, and E. Cambril, Micro-/nanopillars for micro- and nanotechnologies using inductively coupled plasmas, Phys. Status Solidi A **216**, 1900324 (2019).

[40] W. Jo, J. Choi, H. S. Kang, M. Kim, S. Baik, B. J. Lee, C. Pang, and H.-T. Kim, Programmable fabrication of submicrometer bent pillar structures enabled by a photoreconfigurable azopolymer, ACS Appl. Mater. Interfaces **12**, 5058 (2020).

[41] B. Liu, Y. He, P. Fan, and X. Wang, Azo polymer microspherical cap array: Soft-lithographic fabrication and photoinduced shape deformation behavior, Langmuir **23**, 11266 (2007).

[42] F. Fabbri, Y. Lassailly, S. Monaco, K. Lahlil, J. P. Boilot, and J. Peretti, Kinetics of photoinduced matter transport driven by intensity and polarization in thin films containing azobenzene, Phys. Rev. B **86**, 115440 (2012).

[43] Y. Yu, M. Nakano, and T. Ikeda, Directed bending of a polymer film by light, Nature (London) **425**, 145 (2003).

[44] P. Bouchon, C. Koechlin, F. Pardo, R. Haidar, and J.-L. Pelouard, Wideband omnidirectional infrared absorber with a patchwork of plasmonic nanoantennas, Opt. Lett. **37**, 1038 (2012).

[45] H. Sai, T. Matsui, K. Matsubara, M. Kondo, and I. Yoshida, 11.0%-efficient thin-film microcrystalline silicon solar cells with honeycomb textured substrates, IEEE J. Photovoltaics **4**, 1349 (2014).

[46] D. I. Yakubovsky, A. V. Arsenin, Y. V. Stebunov, D. Y. Fedyanin, and V. S. Volkov, Optical constants and structural properties of thin gold films, Opt. Express **25**, 25574 (2017).